Science Advances
AAAS

advances.sciencemag.org/cgi/content/full/6/18/eaaz6579/DC1

# Supplementary Materials for

## Cellular backpacks for macrophage immunotherapy

C. Wyatt Shields IV, Michael A. Evans, Lily Li-Wen Wang, Neil Baugh, Siddharth Iyer, Debra Wu, Zongmin Zhao, Anusha Pusuluri, Anvay Ukidve, Daniel C. Pan, Samir Mitragotri*

*Corresponding author. Email: mitragotri@seas.harvard.edu

Published 29 April 2020, *Sci. Adv.* **6**, eaaz6579 (2020)
DOI: 10.1126/sciadv.aaz6579

**This PDF file includes:**

# I. Supplementary Materials

**Table S1. Antibodies used for flow cytometry.**

| Antibody Target | Fluorophore | Host/Isotype | Clone | Supplier |
|---|---|---|---|---|
| Ly-6G | PE-Cy7 | Rat / IgG2b, kappa | RB6-8C5 | Thermo Fisher Scientific |
| CD11c | PE | Armenian hamster / IgG | N418 | |
| CD11b | FITC | Rat / IgG2b, kappa | M1/70 | |
| CD206 | PE-Cy7 | Rat / IgG2b, kappa | MR6F3 | |
| CD309 (VEGF) | APC | Rat / IgG2a, kappa | Avas12a1 | |
| CD80 | PE | Armenian hamster / IgG | 16-10A1 | |
| MHCII | FITC | Rat / IgG2b, kappa | M5/114.15.2 | |
| iNOS | PE-Cy7 | Rat / IgG2a, kappa | CXNFT | |
| iNOS | APC | Rat / IgG2a, kappa | CXNFT | |
| Isotype Control | PerCP-Cy5.5 | Armenian hamster / IgG | eBio299Arm | |
| Isotype Control | PE-Cy7 | Rat / IgG2a, kappa | eBR2a | |
| Isotype Control | PE | Rat / IgG2a, kappa | eBR2a | |
| Isotype Control | FITC | Rat / IgM, kappa | eBRM | |
| Isotype Control | PerCP-Cy5.5 | Rat / IgG2a, kappa | eBR2a | |
| Isotype Control | PE-Cy7 | Rat / IgG2b, kappa | eB149/10H5 | |
| Isotype Control | PE | Armenian hamster / IgG | eBio299Arm | |
| Isotype Control | FITC | Rat / IgG2b, kappa | eB149/10H5 | |
| Sheep IgG | FITC | Sheep / IgG | Polyclonal | Novus |
| HIF-1α | PE | Rat / IgG1 | 241812 | |
| Arg-1 | FITC | Sheep / IgG | Polyclonal | Fisher Scientific |
| F4/80 | PerCP-Cy5.5 | Rat / IgG2a, kappa | BM8.1 | Millipore Sigma |

## II. Supplementary Methods

**Mold fabrication.** Silicon molds were fabricated using standard monolithic photolithography via methods similar to those described previously (*16*). Briefly, hexamethyldisilazane adhesion promoter was spin-coated on 3" single-side polished silicon wafers (Addison Engineering, Inc.). SPR 220-7.0 (MicroChem Corp.) was spin-coated on each wafer at 4,000 rpm for 45 sec. Wafers underwent a soft bake at 115°C for 90 sec, and were exposed to UV light (405 nm, MA/BA6 Mask Aligner, Süss MicroTec AG) through a chrome-patterned photomask consisting of an array of 8 μm transparent circles with a 16 μm pitch (Photo Sciences, Inc.). Wafers underwent a post-exposure bake at 115°C for 90 sec and were submerged in MF-CD26 for 120 sec. Wafers were cleaned by rinsing with water and drying with a stream of nitrogen gas. Prior to use, molds were passivated with a thin film of trichloro(1H,1H,2H,2H-perfluorooctyl)silane (FDTS) by vapor deposition.

**Synthesis of aldehyde-modified hyaluronic acid (HA-Ald).** HA-Ald was synthesized via methods described previously (*61*). Briefly, sodium hyaluronate (2,500 kDa) was dissolved in 100 mL DI $H_2O$ at 2.5 mg/mL. A 667 μL aliquot of sodium periodate in DI $H_2O$ (10 mg/mL) was added to the HA solution. The mixture was sealed, covered in foil, and vigorously stirred at room temperature. After 2 h, a PBS tablet (Millipore Sigma) was added to the mixture and stirred until fully dissolved. 1,000 mL acetone was then added, precipitating the HA-Ald. The precipitate was collected and pressure was applied to the solid with a spatula to further remove solvent. The precipitate was redissolved in 100 mL of PBS and precipitated again with 1,000 mL of acetone. This entire process was repeated thrice. The precipitate was dissolved in 50−100 mL DI $H_2O$, flash frozen in liquid $N_2$, and lyophilized (SP Scientific Freezemobile Lyophilizer). A sample of the lyophilized solid was analyzed with an FTIR spectrophotometer (Nicolet iS50) to confirm aldehyde modification, as indicated by the appearance of two small sharp peaks between 2,800 and 3,000 $cm^{-1}$ (Fig. S2(A)). These peaks represent stretching of the C-H bonds in the aldehyde functional groups.

**Atomic force microscopy (AFM).** AFM (NanoWizard 4; JPK BioAFM GmbH) was used to characterize the stiffness and morphology of the different layers of the backpack. Layers were individually prepared on polydimethylsiloxane (PDMS) stamps and printed on glass slides treated with plasma for 60 s using methods described in the *Main Text*. A 100 μm cantilever (All-In-One Al; BudgetSensors) with a stiffness of 40 N/m was used in tapping mode. To sample force curves and measure stiffness, a random number generator was used to sample 0.5 μm x 0.5 μm sections of the poly(lactic-co-glycolic acid) (PLGA) disks along their edges. A hertz-fit process was used, assuming a paraboloid tip with 10 nm radius and a Poisson's ratio of 0.265.

**Hypoxia chamber.** A hypoxia chamber (Stemcell Technologies) was used to culture bone marrow derived macrophages (BMDMs) under hypoxic conditions. Prior to incubation, paper towels soaked with PBS were placed along the bottom of the chamber to minimize evaporation. Plates containing BMDMs were sealed with parafilm and placed into the chamber (Parafilm limits evaporation, but allows for gas exchange). The chamber was flushed with a gas mixture containing 94% $N_2$, 5% $CO_2$ and 1% $O_2$ at a flow rate of 20 L/min for 10 min. The chamber was sealed and incubated at 37°C. The chamber was flushed again 2 h later and every 24 h thereafter to ensure consistent oxygen levels.

**Cumulative IFNγ release assay.** After harvesting, backpacks were centrifuged at 1,500xG for 5 min and were reconstituted in BMM- (comprising 500 mL DMEM F12, 50 mL FBS, 5 mL Pen Strep, and 25 mL 200 mM GlutaMAX). Backpacks were counted and diluted to a concentration of $2.0x10^5$ particles/mL. 1 mL sample volumes were transferred to non-stick Eppendorf tubes. For the first time point, each sample was centrifuged at 1,500xG for 5 min. Two 450 μL aliquots were transferred to separate Eppendorf tubes and were frozen at –80°C. 900 μL of fresh BMM- was added to each sample and the sample stored at 37°C until the next time point. The sampling procedure remained the same for all time points, except 925 μL of BMM- was sometimes added after sampling instead of 900 μL to account for liquid evaporation. After the last time point was collected, frozen samples were thawed, diluted 20−50x, and IFNγ concentrations were determined by an ELISA kit. The optical density at 450 nm was recorded using a plate reader (Spectramax i3), following instructions by the manufacturer for background corrections (Molecular Devices, LLC). Standard curves and cumulative IFNγ concentrations were determined in Microsoft Excel.

**Serial dilution.** Due to extensive death of BMDMs from surface tension effects resulting from media removal in 12-well plates, which was reported in other studies (*9*), we utilized a special media exchange technique in wells or dishes with diameters smaller than 60 mm. Instead of aspirating the full liquid volume and adding fresh media, 0.5 mL media was removed from each well (leaving 0.5 mL media in each well), 5 mL of the desired media was added to each well, and then 5 mL of media was removed from each well. This process was repeated a total of two times to nearly replace the original media with the desired media. This procedure is herein referred to as serial dilution.

**Cytokine detection from blood plasma.** Immediately following euthanasia, cardiac punctures were performed to collect blood from mice. Plasma samples were isolated by centrifuging blood samples in gel microtainer tubes at 7,000xG for 1.5 min. Samples were then stored at –80°C until processed for analysis. Serum cytokine levels were quantified using a flow cytometry-based ELISA kit (mouse Th1/Th2/Th17 Cytokine Kit; BD Biosciences) to quantify IL-2, IL-4, IL-6, IFNγ, TNFα, IL-17, and IL-10.

**Immunohistochemical sectioning.** Tumors embedded in OCT compound were cut into 5 μm thick sections using a Leica CM1950 cryostat and mounted on SuperFrost Plus microscope slides (Thermo Fisher). Once dried, slides were washed with PBS twice for 7 min. Slides were fixed with a 3.0 vol.% solution of paraformaldehyde in PBS for 15 min. Slides were washed once with PBS for 7 min. Slides were then mounted with ProLong Diamond antifade mountant with DAPI following instructions from the manufacturer (Thermo Fisher). 24 h later, slides were sealed with nail polish and stored at −20°C until imaging. Sections were analyzed with a Zeiss Axio Scan.Z1 Slide Scanner Microscope (10x objective). Images were processed with ImageJ.

## III. Supplementary Figures

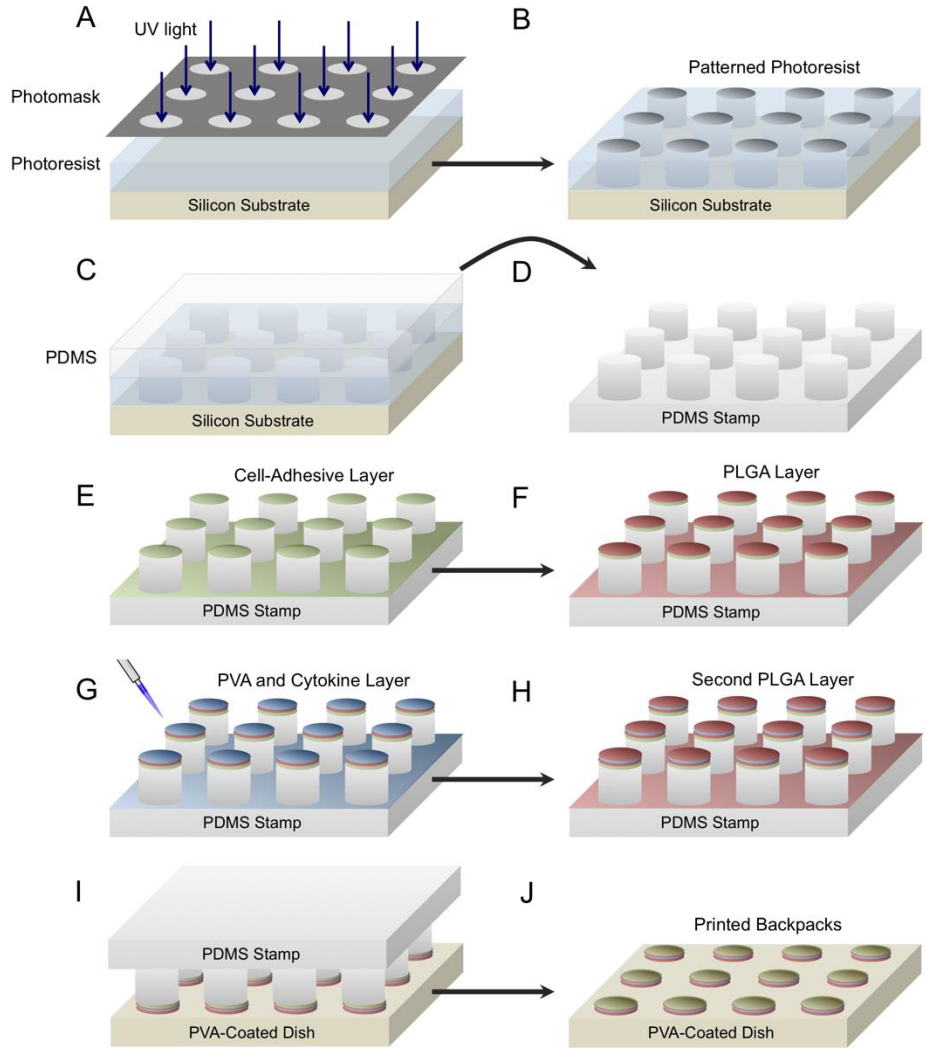


**Fig. S1. Fabrication of IFNγ backpacks.** (A) Silicon molds were prepared by photolithography. (B) Molds contained an array of cylindrical holes, 8 μm across and 7 μm deep, with a pitch of 16 μm. Completed molds were treated with FDTS by vapor deposition. (C) Polydimethylsiloxane (PDMS) was poured over the molds, degassed, and cured. (D) PDMS was separated from the mold, forming a stamp. (E) PDMS stamps were coated with alternating layers of charged, cell-adhesive polymers. (F) A poly(lactic-co-glycolic acid) (PLGA) solution was spin coated over the stamps. (G) Stamps were plasma ashed, coated with an aqueous film of poly(vinyl alcohol) (PVA) containing IFNγ, and were dried by evaporation. (H) A second PLGA solution was spin coated over the stamps. (I) PVA-coated dishes were heated over a water bath. (J) PDMS stamps were pressed onto the dishes to transfer an array of the IFNγ backpacks by microcontact printing. See *Methods Section* for details on backpack fabrication.

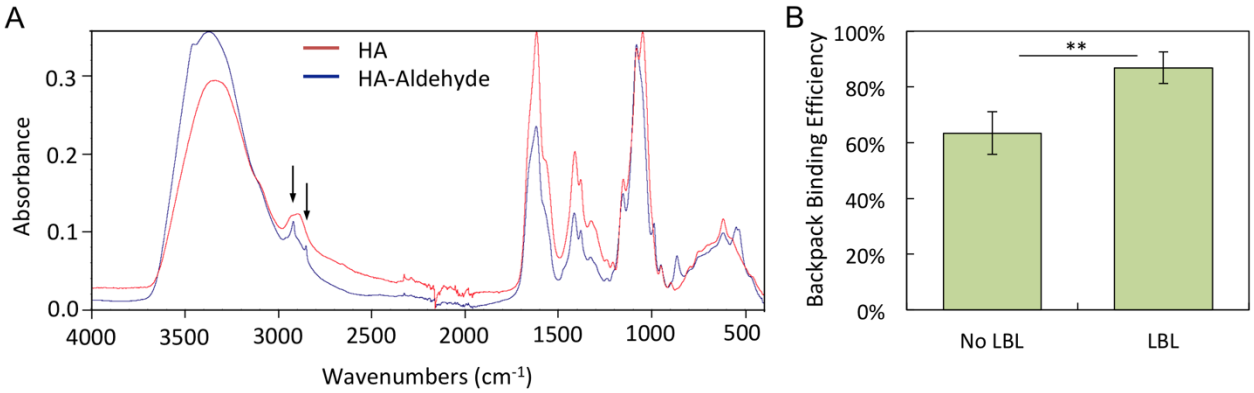


**Fig. S2. Characterization of the layer-by-layer (LBL) coating.** (A) FTIR spectra of HA (red) and HA-Ald (blue). Aldehyde modification is confirmed by the appearance of the two small sharp peaks between 2,800 and 3,000 $cm^{-1}$ (arrows). (B) Binding efficiency of backpacks to primary BMDMs (see Methods in the *Main Text* for binding procedures). Efficiency is defined as number of cells with >1 backpack, as determined by flow cytometry (n = 5).

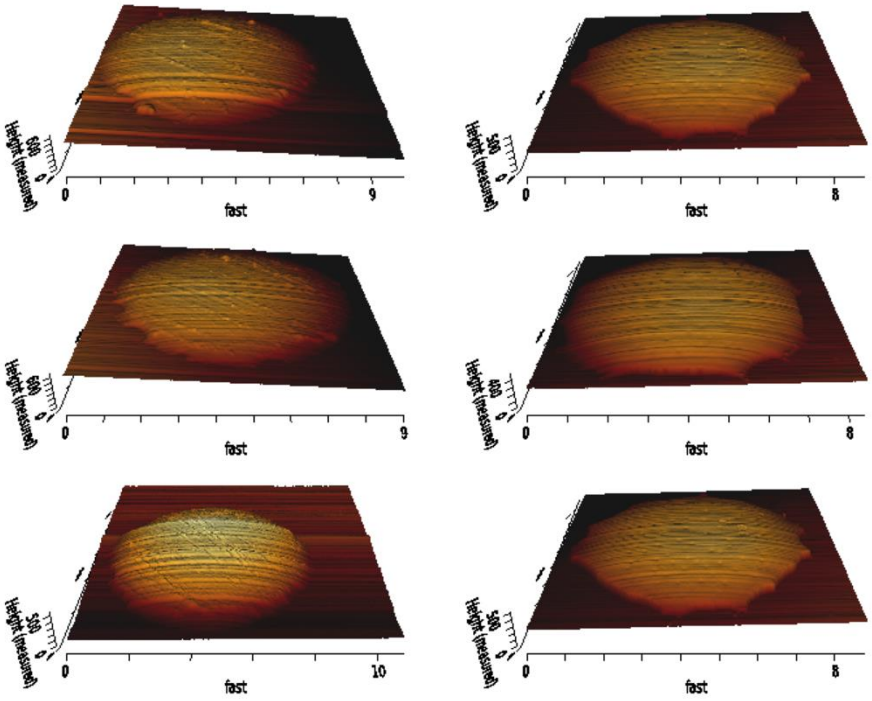


**Fig. S3. AFM images of PLGA discs.** Six representative topographical images of single PLGA discs produced by AFM. The average thickness of the backpacks shown in Fig. 2A(iii) was determined by separately measuring the thickness of each layer of the backpacks via AFM and adding. We note that the PVA layer could not be measured by AFM, so the thickness of the PVA layer was estimated using a simple density calculation.

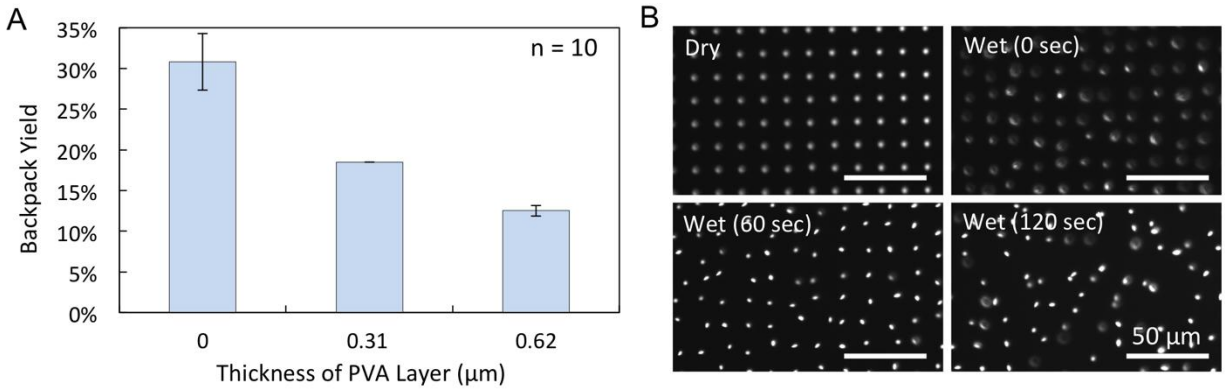


**Fig. S4. Printing and release of backpacks.** (A) Backpacks were made and printed that comprised two layers of PLGA encasing a PVA layer of 0 μm (no PVA), 0.31 μm and 0.62 μm thickness (n = 10). The PVA layer was made by depositing and subsequently drying a 100 μL solution of 0, 0.25 and 0.50 vol.% PVA in PBS, respectively, on a 25 mm x 25 mm PDMS stamp (Fig. S1). Printing efficiency was determined by a hemocytometer after backpacks were suspended. (B) Images depicting a printed array of backpacks released from a substrate after the addition of PBS. Backpacks in (B) comprised of a single layer of PLGA, which has a higher printing efficiency than those described in (A).

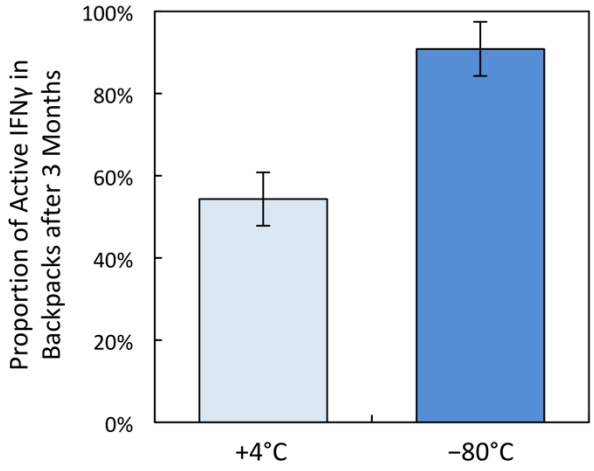


**Fig. S5. Stability of encapsulated IFNγ. IFNγ backpacks were printed and stored at 4°C or −80°C for 3 months.** IFNγ was extracted from the backpacks using the cumulative release assay (see Methods in the *Main Text*) and quantified by ELISA. Proportion of active IFNγ content was determined via comparison to averaged values from the same assay performed on backpacks immediately after fabrication ($n \geq 6$).

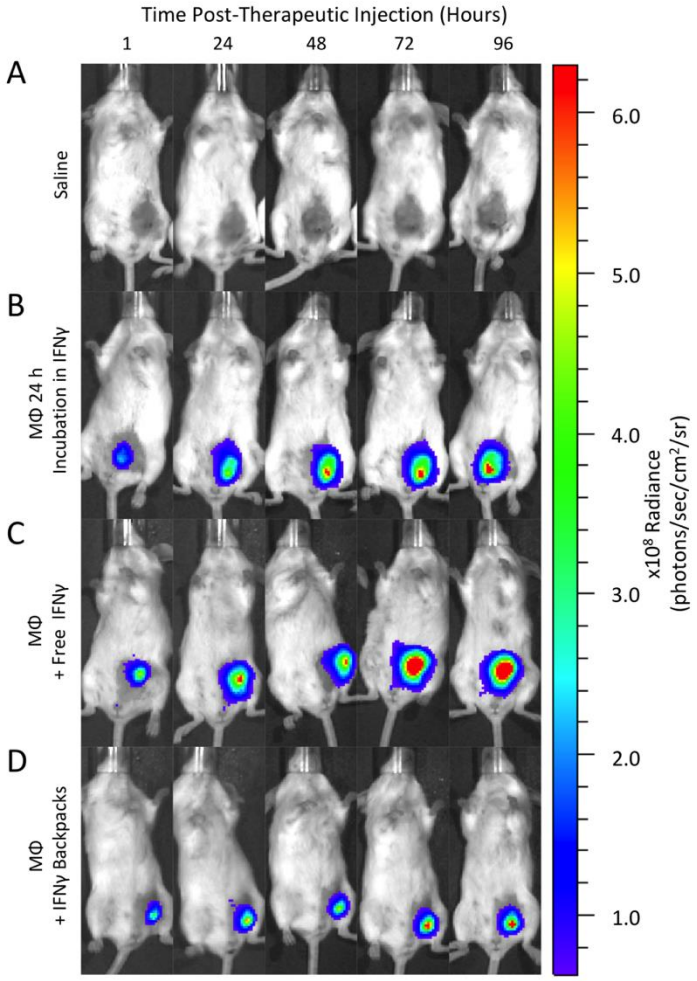


**Fig. S6. Intratumoral distribution of injected macrophages (MΦs) after a single injection.** Grayscale images with overlaid recordings of average radiance, as determined by an *in vivo* imaging system (IVIS), of mice injected with: (A) saline and (B−D) MΦs labeled with VivoTrack 680 near-infrared dye. Prior to injection, MΦs were (B) polarized *ex vivo* for 24 h with 16 ng/mL IFNγ (MΦ 24 h incubation in IFNγ), (C) left unpolarized and mixed with 50 ng free IFNγ immediately prior to injection (MΦ + free IFNγ), and (D) left unpolarized and bound to IFNγ backpacks at a concentration of 50 ng equivalent IFNγ immediately prior to injection (MΦ + IFNγ backpacks).

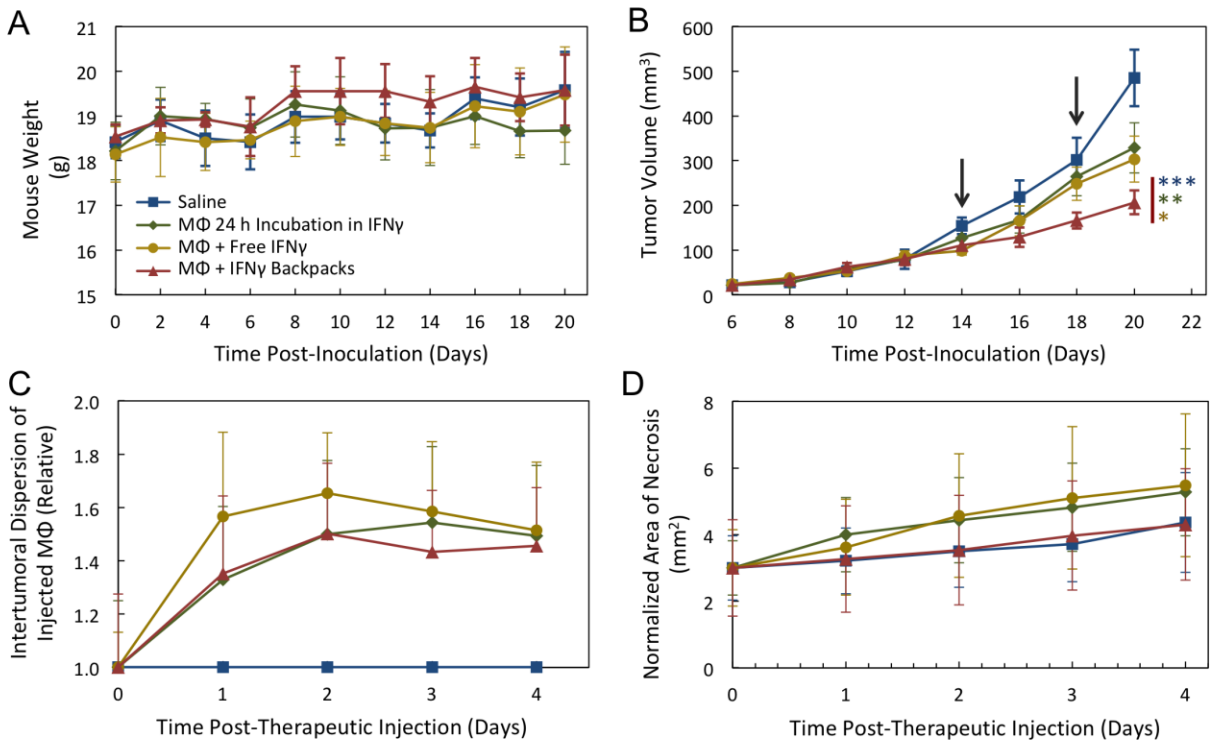


**Fig. S7. Efficacy of IFNγ backpacks to treat BALB/c mice with 4T1 triple negative breast carcinomas.** Prior to injection, macrophages (MΦs) were (i) left unpolarized (saline, blue), (ii) polarized *ex vivo* for 24 h with 16 ng/mL IFNγ (MΦ 24 h incubation in IFNγ, green), (iii) left unpolarized and mixed with 50 ng free IFNγ immediately prior to injection (MΦ + free IFNγ, yellow) and (iv) left unpolarized and bound to IFNγ backpacks at a concentration of 50 ng equivalent IFNγ immediately prior to injection (MΦ + IFNγ backpacks, red). (A) Average mouse body weight in all groups. (B) Tumor growth curves for all groups. Solid arrows indicate days of intratumoral injections. (C) Distribution of injected MΦs relative to their distribution immediately after injection, as determined by an IVIS (raw images in Fig. S6). (D) Progression of necrosis. Photographs of tumors on dehaired mice were taken each day after the first injection. To evaluate if the treatment group altered the rate of necrosis, the average area of necrosis was determined for each group by ImageJ (NIH) and normalized to the first day. No significant differences were observed. Time in (C) and (D) is with respect to the first therapeutic injection (n = 5 for all graphs)

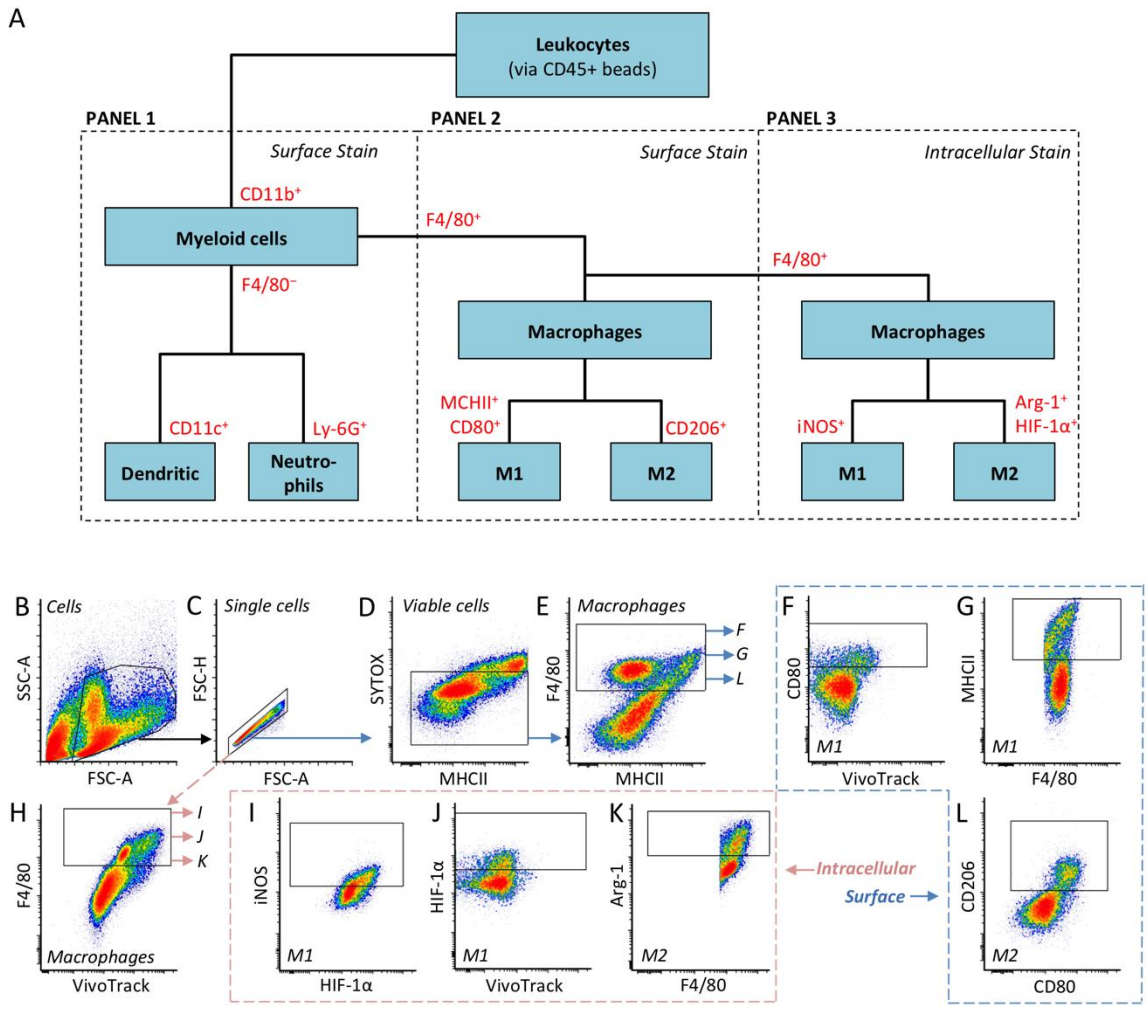


**Fig. S8. Phenotyping tumor-associated immune cells.** (A) Panel organization for phenotyping tumor-associated immune cells from orthotopic 4T1 breast tumors. Tumor-associated leukocytes were split into 3 panels for separate staining and inspection by flow cytometry, as demarcated by the dotted grey boxes. Phenotypic markers used for identifying different cell populations are shown in red text. Corresponding isotype controls are listed in *Table S1*. (B−L) Gating schema for phenotyping TAMs by flow cytometry. Hierarchical gates were drawn for (B) cells, (C) single cells, (D) viable cells and then (E) macrophages. Subplots were drawn from (E) to stain for (F) CD80, (G) MHCII and (L) CD206 on cellular surfaces (light blue dotted lines). To stain for intracellular markers, a subplot was drawn from (C) to identify viable and non-viable macrophages (H). From (H), subplots were drawn for (I) iNOS, (J) HIF-1α and (K) Arg-1 (pink dotted lines). Figure 4B in the *Main Text* displays the relative change in the median intensity for (F, G, I, J, L and K). We note that the same schema was used for phenotyping injected macrophages, with the additional criteria of gating for macrophages stained with VivoTrack 680 near-infrared dye.

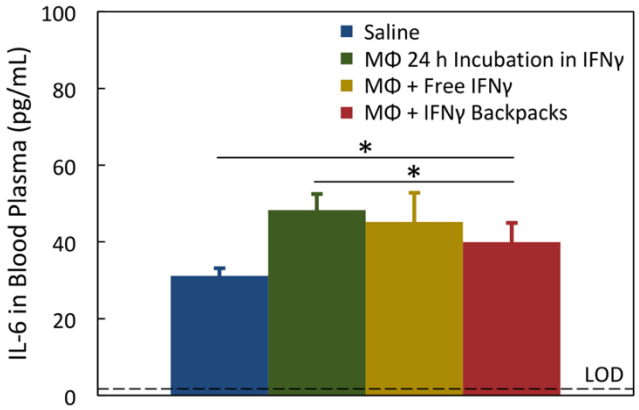


**Fig. S9. IL-6 concentration in blood plasma.** IL-6 was measured in the plasma of 4T1 tumor-bearing mice treated with: (i) saline, blue; (ii) macrophages (MΦ) treated 24 h in 20 ng/mL IFNγ, green; (iii) MΦ with 50 ng free IFNγ, yellow; and (iv) MΦ bound to IFNγ-loaded backpacks, red (n = 5). Blood plasma of IL-2, IL-4, IFNγ, TNFα, IL-17 and IL-10 was also measured, but was below the limit of detection.

## REFERENCES


1. D. N. Khalil, E. L. Smith, R. J. Brentjens, J. D. Wolchok, The future of cancer treatment: Immunomodulation, CARs and combination immunotherapy. *Nat. Rev. Clin. Oncol.* **13**, 273–290 (2016).

2. A. N. Miliotou, L. C. Papadopoulou, CAR T-cell therapy: A new era in cancer immunotherapy. *Curr. Pharm. Biotechnol.* **19**, 5–18 (2018).

3. G. Hucks, S. R. Rheingold, The journey to CAR T cell therapy: The pediatric and young adult experience with relapsed or refractory B-ALL. *Blood Cancer J.* **9**, 10 (2019).

4. S. Lee, S. Kivimäe, A. Dolor, F. C. Szoka, Macrophage-based cell therapies: The long and winding road. *J. Control. Release* **240**, 527–540 (2016).

5. T. A. Wynn, A. Chawla, J. W. Pollard, Macrophage biology in development, homeostasis and disease. *Nature* **496**, 445–455 (2013).

6. F. O. Martinez, S. Gordon, The M1 and M2 paradigm of macrophage activation: Time for reassessment. *F1000Prime Rep.* **6**, 13 (2014).

7. J. M. Brown, L. Recht, S. Strober, The Promise of Targeting Macrophages in Cancer Therapy. *Clin. Cancer Res.* **23**, 3241–3250 (2017).

8. J. L. Schultze, A. Schmieder, S. Goerdt, Macrophage activation in human diseases. *Semin. Immunol.* **27**, 249–256 (2015).

9. M. A. Evans, P. J. Huang, Y. Iwamoto, K. N. Ibsen, E. M. Chan, Y. Hitomi, P. C. Ford, S. Mitragotri, Macrophage-mediated delivery of light activated nitric oxide prodrugs with spatial, temporal and concentration control. *Chem. Sci.* **9**, 3729–3741 (2018).

10. C. B. Williams, E. S. Yeh, A. C. Soloff, Tumor-associated macrophages: Unwitting accomplices in breast cancer malignancy. *NPJ Breast Cancer* **2**, 15025 (2016).

11. J. A. Champion, S. Mitragotri, Role of target geometry in phagocytosis. *Proc. Natl. Acad. Sci. U.S.A.* **103**, 4930–4934 (2006).

12. N. Doshi, A. J. Swiston, J. B. Gilbert, M. L. Alcaraz, R. E. Cohen, M. F. Rubner, S. Mitragotri, Cell-based drug delivery devices using phagocytosis-resistant backpacks. *Adv. Mater.* **23**, H105–H109 (2011).

13. A. C. Anselmo, J. B. Gilbert, S. Kumar, V. Gupta, R. E. Cohen, M. F. Rubner, S. Mitragotri, Monocyte-mediated delivery of polymeric backpacks to inflamed tissues: A generalized strategy to deliver drugs to treat inflammation. *J. Control. Release* **199**, 29–36 (2015).

14. J. Xia, Z. Wang, D. Huang, Y. Yan, Y. Li, J. Guan, Asymmetric biodegradable microdevices for cell-borne drug delivery. *ACS Appl. Mater. Interfaces* **7**, 6293–6299 (2015).

15. N. L. Klyachko, R. Polak, M. J. Haney, Y. Zhao, R. J. Gomes Neto, M. C. Hill, A. V. Kabanov, R. E. Cohen, M. F. Rubner, E. V. Batrakova, Macrophages with cellular backpacks for targeted drug delivery to the brain. *Biomaterials* **140**, 79–87 (2017).

16. P. Zhang, J. Guan, Fabrication of multilayered microparticles by integrating layer-by-layer assembly and microcontact printing. *Small* **7**, 2998–3004 (2011).

17. B. Huang, W. D. Abraham, Y. Zheng, S. C. Bustamante López, S. S. Luo, D. J. Irvine, Active targeting of chemotherapy to disseminated tumors using nanoparticle-carrying T cells. *Sci. Transl. Med.* **7**, 291ra294 (2015).

18. L. Tang, Y. Zheng, M. B. Melo, L. Mabardi, A. P. Castaño, Y.-Q. Xie, N. Li, S. B. Kudchodkar, H. C. Wong, E. K. Jeng, M. V. Maus, D. J. Irvine, Enhancing T cell therapy through TCR-signaling-responsive nanoparticle drug delivery. *Nat. Biotechnol.* **36**, 707–716 (2018).

19. C. W. Shields IV, L. L.-W. Wang, M. A. Evans, S. Mitragotri, Materials for Immunotherapy. *Adv. Mater.* **2019**, e1901633 (2019).

20. K. Schroder, P. J. Hertzog, T. Ravasi, D. A. Hume, Interferon-γ: An overview of signals, mechanisms and functions. *J. Leukoc. Biol.* **75**, 163–189 (2004).

21. F. C. Vasconcellos, A. J. Swiston, M. M. Beppu, R. E. Cohen, M. F. Rubner, Bioactive polyelectrolyte multilayers: Hyaluronic acid mediated B lymphocyte adhesion. *Biomacromolecules* **11**, 2407–2414 (2010).

22. P. Tripathi, P. Tripathi, L. Kashyap, V. Singh, The role of nitric oxide in inflammatory reactions. *FEMS Immunol. Med. Microbiol.* **51**, 443–452 (2007).

23. V. Steimle, C. Siegrist, A. Mottet, B. Lisowska-Grospierre, B. Mach, Regulation of MHC class II expression by interferon-gamma mediated by the transactivator gene CIITA. *Science* **265**, 106–109 (1994).

24. C. Wu, Y. Xue, P. Wang, L. Lin, Q. Liu, N. Li, J. Xu, X. Cao, IFN-γ primes macrophage activation by increasing phosphatase and tensin homolog via downregulation of miR-3473b. *J. Immunol.* **193**, 3036–3044 (2014).

25. A. M. Labrousse, E. Meunier, J. Record, A. Labernadie, A. Beduer, C. Vieu, T. Ben Safta, I. Maridonneau-Parini, Frustrated phagocytosis on micro-patterned immune complexes to characterize lysosome movements in live macrophages. *Front. Immunol.* **2**, 51 (2011).

26. A. Mularski, F. Marie-Anaïs, J. Mazzolini, F. Niedergang, *Observing Frustrated Phagocytosis and Phagosome Formation and Closure Using Total Internal Reflection Fluorescence Microscopy (TIRFM)*, G. Rousselet, Ed. (Humana Press New York, NY, 2018).

27. K. Mittal, J. Ebos, B. Rini, Angiogenesis and the tumor microenvironment: vascular endothelial growth factor and beyond. *Semin. Oncol.* **41**, 235–251 (2014).

28. A. L. Doedens, C. Stockmann, M. P. Rubinstein, D. Liao, N. Zhang, D. G. DeNardo, L. M. Coussens, M. Karin, A. W. Goldrath, R. S. Johnson, Macrophage expression of hypoxia-inducible factor-1 alpha suppresses T-cell function and promotes tumor progression. *Cancer Res.* **70**, 7465–7475 (2010).

29. P. Scodeller, L. Simón-Gracia, S. Kopanchuk, A. Tobi, K. Kilk, P. Säälik, K. Kurm, M. L. Squadrito, V. R. Kotamraju, A. Rinken, M. de Palma, E. Ruoslahti, T. Teesalu, Precision Targeting of Tumor Macrophages with a CD206 Binding Peptide. *Sci. Rep.* **7**, 14655 (2017).

30. A. Pusuluri, V. Krishnan, D. Wu, C. W. Shields IV, L. W. Wang, S. Mitragotri, Role of synergy and immunostimulation in design of chemotherapy combinations: An analysis of doxorubicin and camptothecin. *Bioeng. Transl. Med.* **4**, e10129 (2019).

31. R. Deng, S. M. Wang, T. Yin, T. H. Ye, G. B. Shen, L. Li, J. Y. Zhao, Y. X. Sang, X. G. Duan, Y. Q. Wei, Inhibition of tumor growth and alteration of associated macrophage cell type by an HO-1 inhibitor in breast carcinoma-bearing mice. *Oncol. Res.* **20**, 473–482 (2012).

32. W. Durante, F. K. Johnson, R. A. Johnson, Arginase: A critical regulator of nitric oxide synthesis and vascular function. *Clin. Exp. Pharmacol. Physiol.* **34**, 906–911 (2007).

33. C. Perrotta, D. Cervia, I. di Renzo, C. Moscheni, M. T. Bassi, L. Campana, C. Martelli, E. Catalani, M. Giovarelli, S. Zecchini, M. Coazzoli, A. Capobianco, L. Ottobrini, G. Lucignani, P. Rosa, P. Rovere-Querini, C. de Palma, E. Clementi, Nitric oxide generated by tumor-associated macrophages is responsible for cancer resistance to cisplatin and correlated with syntaxin 4 and acid sphingomyelinase inhibition. *Front. Immunol.* **9**, 1186 (2018).

34. Y. W. Choo, M. Kang, H. Y. Kim, J. Han, S. Kang, J. R. Lee, G. J. Jeong, S. P. Kwon, S. Y. Song, S. Go, M. Jung, J. Hong, B. S. Kim, M1 macrophage-derived nanovesicles potentiate the anticancer efficacy of immune checkpoint inhibitors. *ACS Nano* **12**, 8977–8993 (2018).

35. Y. Wang, Y.-X. Lin, S.-L. Qiao, H.-W. An, Y. Ma, Z.-Y. Qiao, R. P. Y. J. Rajapaksha, H. Wang, Polymeric nanoparticles promote macrophage reversal from M2 to M1 phenotypes in the tumor microenvironment. *Biomaterials* **112**, 153–163 (2017).

36. M. Song, T. Liu, C. Shi, X. Zhang, X. Chen, Bioconjugated manganese dioxide nanoparticles enhance chemotherapy response by priming tumor-associated macrophages toward m1-like phenotype and attenuating tumor hypoxia. *ACS Nano* **10**, 633–647 (2016).

37. S. Zanganeh, G. Hutter, R. Spitler, O. Lenkov, M. Mahmoudi, A. Shaw, J. S. Pajarinen, H. Nejadnik, S. Goodman, M. Moseley, L. M. Coussens, H. E. Daldrup-Link, Iron oxide nanoparticles inhibit tumour growth by inducing pro-inflammatory macrophage polarization in tumour tissues. *Nat. Nanotechnol.* **11**, 986–994 (2016).

38. J. L. Guerriero, A. Sotayo, H. E. Ponichtera, J. A. Castrillon, A. L. Pourzia, S. Schad, S. F. Johnson, R. D. Carrasco, S. Lazo, R. T. Bronson, S. P. Davis, M. Lobera, M. A. Nolan, A. Letai, Class IIa HDAC inhibition reduces breast tumours and metastases through anti-tumour macrophages. *Nature* **543**, 428–432 (2017).

39. C.-X. Li, Y. Zhang, X. Dong, L. Zhang, M.-D. Liu, B. Li, M.-K. Zhang, J. Feng, X.-Z. Zhang, Artificially reprogrammed macrophages as tumor-tropic immunosuppression-resistant biologics to realize therapeutics production and immune activation. *Adv. Mater.* **31**, e1807211 (2019).

40. S. Edin, M. L. Wikberg, A. M. Dahlin, J. Rutegård, Å. Öberg, P. A. Oldenborg, R. Palmqvist, The distribution of macrophages with a M1 or M2 phenotype in relation to prognosis and the molecular characteristics of colorectal cancer. *PLOS ONE* **7**, e47045 (2012).

41. A. Yuan, Y.-J. Hsiao, H.-Y. Chen, H.-W. Chen, C.-C. Ho, Y.-Y. Chen, Y.-C. Liu, T.-H. Hong, S.-L. Yu, J. J.-W. Chen, P.-C. Yang, Opposite effects of M1 and M2 macrophage subtypes on lung cancer progression. *Sci. Rep.* **5**, 14273 (2015).

42. Y. Zhang, S. Cheng, M. Zhang, L. Zhen, D. Pang, Q. Zhang, Z. Li, High-infiltration of tumor-associated macrophages predicts unfavorable clinical outcome for node-negative breast cancer. *PLOS ONE* **8**, e76147 (2013).

43. C. D. Mills, L. L. Lenz, R. A. Harris, A Breakthrough: Macrophage-Directed Cancer Immunotherapy. *Cancer Res.* **76**, 513–516 (2016).

44. T. O'Sullivan, R. Saddawi-Konefka, W. Vermi, C. M. Koebel, C. Arthur, J. M. White, R. Uppaluri, D. M. Andrews, S. F. Ngiow, M. W. Teng, M. J. Smyth, R. D. Schreiber, J. D. Bui, Cancer immunoediting by the innate immune system in the absence of adaptive immunity. *J. Exp. Med.* **209**, 1869–1882 (2012).

45. L. F. Tremble, P. F. Forde, D. M. Soden, Clinical evaluation of macrophages in cancer: role in treatment, modulation and challenges. *Cancer Immunol. Immunother.* **66**, 1509–1527 (2017).

46. A. Ramesh, S. Kumar, D. Nandi, A. Kulkarni, CSF1R- and SHP2-inhibitor-loaded nanoparticles enhance cytotoxic activity and phagocytosis in tumor-associated macrophages. *Adv Mater* **31**, e1904364 (2019).

47. N. N. Parayath, A. Parikh, M. M. Amiji, Repolarization of tumor-associated macrophages in a genetically engineered nonsmall cell lung cancer model by intraperitoneal administration of hyaluronic acid-based nanoparticles encapsulating MicroRNA-125b. *Nano Lett.* **18**, 3571–3579 (2018).

48. Y. Liu, X. Liang, X. Yin, J. Lv, K. Tang, J. Ma, T. Ji, H. Zhang, W. Dong, X. Jin, D. Chen, Y. Li, S. Zhang, H. Q. Xie, B. Zhao, T. Zhao, J. Lu, Z. W. Hu, X. Cao, F. X. F. Qin, B. Huang, Blockade of IDO-kynurenine-AhR metabolic circuitry abrogates IFN-γ-induced immunologic dormancy of tumor-repopulating cells. *Nat. Commun.* **8**, 15207 (2017).

49. C. H. Miller, S. G. Maher, H. A. Young, Clinical Use of Interferon-gamma. *Ann. N. Y. Acad. Sci.* **1182**, 69–79 (2009).

50. G. L. Razidlo, K. M. Burton, M. A. McNiven, Interleukin-6 promotes pancreatic cancer cell migration by rapidly activating the small GTPase CDC42. *J. Biol. Chem.* **293**, 11143–11153 (2018).

51. G. Arango Duque, A. Descoteaux, Macrophage cytokines: Involvement in immunity and infectious diseases. *Front. Immunol.* **5**, 491 (2014).

52. B. M. Carreno, V. Magrini, M. Becker-Hapak, S. Kaabinejadian, J. Hundal, A. A. Petti, A. Ly, W. R. Lie, W. H. Hildebrand, E. R. Mardis, G. P. Linette, A dendritic cell vaccine increases the breadth and diversity of melanoma neoantigen-specific T cells. *Science* **348**, 803–808 (2015).

53. T. Wang, D. Wang, H. Yu, B. Feng, F. Zhou, H. Zhang, L. Zhou, S. Jiao, Y. Li, A cancer vaccine-mediated postoperative immunotherapy for recurrent and metastatic tumors. *Nat. Commun.* **9**, 1532 (2018).

54. A. S. Cheung, D. K. Y. Zhang, S. T. Koshy, D. J. Mooney, Scaffolds that mimic antigen-presenting cells enable ex vivo expansion of primary T cells. *Nat. Biotechnol.* **36**, 160–169 (2018).

55. H. I. Tong, W. Kang, P. M. C. Davy, Y. Shi, S. Sun, R. C. Allsopp, Y. Lu, Monocyte trafficking, engraftment, and delivery of nanoparticles and an exogenous gene into the acutely inflamed brain tissue - evaluations on monocyte-based delivery system for the central nervous system. *PLOS ONE* **11**, e0154022 (2016).

56. T. M. Raimondo, D. J. Mooney, Functional muscle recovery with nanoparticle-directed M2 macrophage polarization in mice. *Proc. Natl. Acad. Sci. U.S.A.* **115**, 10648–10653 (2018).

57. M.-A. Shahbazi, M. Sedighi, T. Bauleth-Ramos, K. Kant, A. Correia, N. Poursina, B. Sarmento, J. Hirvonen, H. A. Santos, Targeted reinforcement of macrophage reprogramming toward M2 polarization by IL-4-loaded hyaluronic acid particles. *ACS Omega* **3**, 18444–18455 (2018).

58. X. Zhang, R. Goncalves, D. M. Mosser, The isolation and characterization of murine macrophages. *Curr. Protoc. Immunol.* **Chapter 14**, Unit 14.1 (2008).

59. R. Andreesen, C. Scheibenbogen, W. Brugger, S. Krause, H. G. Meerpohl, H. G. Leser, H. Engler, G. W. Löhr, Adoptive transfer of tumor cytotoxic macrophages generated in vitro from circulating blood monocytes: A new approach to cancer immunotherapy. *Cancer Res.* **50**, 7450–7456 (1990).

60. M. Weis, J. Shan, M. Kuhlmann, T. Jungst, J. Tessmar, J. Groll, Evaluation of hydrogels based on oxidized hyaluronic acid for bioprinting. *Gels* **4**, E82 (2018).